

# Identifying the Lens Galaxy B 1152+199 as a Ghostly Damped Lyman Alpha System by the Cosmic Origin Spectrograph

Xinyu Dai<sup>1</sup> and Bin Chen<sup>2</sup>

## ABSTRACT

Strong quasar-galaxy lensing provides a powerful tool to probe the inter-stellar medium (ISM) of the lens galaxy using radiation from the background quasar. Using the Cosmic Origin Spectrograph (COS) on board the Hubble Space Telescope, we study the cold ISM properties of the lens galaxy in B 1152+199 at a redshift of  $z = 0.4377$ . Since existing optical extinction and X-ray absorption measurements of the lens have revealed a large amount of cold ISM, we expected to detect a damped Ly $\alpha$  absorption (DLA) system in the near ultraviolet spectrum; however, our upper limit on the H I column density is several orders of magnitude below the expectation. We also marginally detect O I and C II absorption lines associated with the lens galaxy in the COS spectrum. Thus, the lens galaxy is identified as a ghostly DLA system, and further investigations of these ghostly DLA systems would be important to characterize the biases of using DLAs to probe the matter density of the universe. Although preliminary, the most likely explanation of the non-detection of the DLA is because of the Ly $\alpha$  emission of the lens galaxy that fills in the absorption trough, with a Ly $\alpha$  luminosity of  $4 \times 10^{42}$  erg s<sup>-1</sup>.

*Subject headings:* gravitational lensing: strong — galaxies: ISM — galaxies: individual (B 1152+199) — ultraviolet: ISM

## 1. Introduction

The inter-stellar medium (ISM) has a primary role in many areas of astronomy, including stellar formation/evolution, galaxy formation/evolution, physics of active galactic nuclei, and

---

<sup>1</sup>Homer L. Dodge Department of Physics and Astronomy, University of Oklahoma, Norman, OK, 73019, USA, xdai@ou.edu

<sup>2</sup>Research Computing Center, Department of Scientific Computing, Florida State University, Tallahassee, Florida 32306, USA

cosmology. Quasar-galaxy strong gravitational lensing systems form a powerful tool to study the ISM properties of intermediate redshift galaxies. Here, a bright background quasar lies with a small impact parameter behind a foreground galaxy (most lens galaxies are elliptical), and multiple images form due to the gravitational lensing effect. Because of the small impact parameter, the quasar light traverses the ISM of the lens galaxy, and the cold ISM leaves signatures on the lensed quasar spectrum, including reddening due to dust, absorption of the X-ray spectrum, and absorption lines in the ultraviolet (UV) and optical bands. This method is unique in its ability to probe ISM of high density regions deep within the lens galaxy. Most absorption line systems probe lines of sight far more distant from the galaxy center (e.g., Prochaska & Herbert-Fort 2004; Ménard & Chelouche 2009). Future large-scale surveys, such as the Large Synoptic Survey Telescope, will find thousands of strong quasar-galaxy lenses (Oguri & Marshall 2010) that can be used for ISM studies.

The first two effects, dust extinction and X-ray absorption, have been investigated in the literature. For example, extinction laws of intermediate redshift galaxies has been studied in many gravitational lenses (e.g., Nadeau et al. 1991; Falco et al. 1999; Toft, Hjorth & Burud 2000; Motta et al. 2002; Wucknitz et al. 2003; Muñoz et al. 2004; Mediavilla et al. 2005). Gravitational lenses also provide the first probes capable of studying the dust-to-gas ratios of cosmologically distant galaxies (Dai et al. 2003; Dai & Kochanek 2005; Dai et al. 2006; Dai & Kochanek 2009). By combining X-ray and optical measurements of both the gas and dust absorption between pairs of lensed images, we can estimate the dust-to-gas ratio  $\Delta E(B - V)/\Delta N_{\text{H}}$  of the lens galaxies, under the assumption that the differences between the extinction and gas absorption are due to the same parcel of ISM. Chen et al. (2013) found an evolving dust-to-gas ratio of  $E(B - V)/N_{\text{H}} = 1.17_{-0.31}^{+0.41} \times 10^{-22} \text{ mag cm}^2 \text{ atom}^{-1}$  in lens galaxies ( $0 < z < 1$ ), with an intrinsic scatter of 0.3 dex, lower than the Galactic value  $1.7 \times 10^{-22} \text{ mag cm}^2 \text{ atom}^{-1}$  (Bohlin, Savage & Drake 1978), and a constant dust-to-metal ratio with redshift.

This paper focuses on the hydrogen and metal absorption lines in a UV spectrum of the lens galaxy in the two-image lens B 1152+199. B 1152+199 was selected as a lens candidate from the Cosmic Lens All-Sky Survey, and was confirmed as a two-image lens system with  $z_s = 1.019$  and  $z_l = 0.439$  by subsequent follow-up observations (Myers et al. 1999). The *HST* F555W and F814W band images of B 1152+199 show that the lensing galaxy may resemble an early-type galaxy (Rusin et al. 2002). However, the large amount of cold ISM detected from the lens galaxy, through studying the absorption/extinction properties of the background quasar spectrum, will classify the galaxy as a late-type. In particular, Myers et al. (1999) detected Mg II and Mg I metal absorption lines at the lens redshift from the optical spectrum of the quasar image A (C. Fassnacht, private communication). Toft, Hjorth & Burud (2000) detected a large extinction for the system, especially in quasar

image B, and Elíasdóttir et al. (2006) confirmed this result and measured a large differential extinction of  $\Delta E(B - V) = 1.20 \pm 0.05$  between images A and B with a slope of  $R_V = 2.1 \pm 0.1$ . Dai & Kochanek (2009) and Chen et al. (2013) detected cold ISM in the lens from X-ray spectra of the quasar images and measured differential absorption of  $\Delta N_{\text{H}} = (4.8 \pm 0.4) \times 10^{22} \text{ cm}^{-2}$  assuming Solar metallicity. Combining the differential extinction and absorption measurements, Dai & Kochanek (2009) measured a dust-to-gas ratio of  $E(B - V)/N_{\text{H}} = (2.5 \pm 0.2) \times 10^{-22} \text{ mag cm}^2 \text{ atom}^{-1}$ , slightly higher than the Galactic value  $1.7 \times 10^{-22} \text{ mag cm}^2 \text{ atom}^{-1}$  (Bohlin, Savage & Drake 1978).

Since metals dominate the X-ray absorption cross section, the  $N_{\text{H}}$  measured from the X-ray spectrum is an effective column density rather than a direct measurement. Ideally a direct measurement of  $N_{\text{H}}$  using other methods can be vital to break the degeneracy in the X-ray analysis. The original goal of our Cosmic Origin Spectrograph (COS) observation of B 1152+199 was to directly measure  $N_{\text{H}}$  through the damped Ly $\alpha$  absorption (DLA) feature associated with the lens galaxy and also to detect other associated metal absorption lines in the brighter image A. Here, we present the non-detection of the DLA in B 1152+199. The observation and data products are introduced in Section 2, followed by the imaging analysis in Section 3 and the spectral analysis in Section 4. We discuss the results in Section 5. We assume cosmological parameters of  $\Omega_M = 0.27$ ,  $\Omega_\Lambda = 0.73$ , and  $H_0 = 70 \text{ km s}^{-1} \text{ Mpc}^{-1}$  throughout the paper.

## 2. Observation

We obtained a low-resolution NUV spectrum of B 1152+199 using COS (Green et al. 2012) onboard *HST* with the G230L grating on 2014-04-15. We used two central wavelengths to cover a broader wavelength range and four positions for each central wavelength to minimize any local systematics in the detector, such as the bad pixels. The detailed observation log is listed in Table 1. The data products were retrieved from STScI after updating the wavelength calibration issue in the G230L grating mode in May 2016, and we used the standard pipeline-produced, background-subtracted spectrum in our subsequent analysis.

## 3. Imaging Analysis

We analyzed the acquisition image of B 1152+199, taken with the COS/NUV/MirrorB configuration with an exposure of 95.6 sec, and only detected image A. Although two point sources were detected, they are the double-image caused by MirrorB. We first modeled the

Table 1. *HST*-COS Observations of B 1152+199.

Target	Instrument	Grating	Wavelength Coverage (Å)	Spectral Resolution <sup>a</sup>	Exposure Time (sec)
B 1152+199	COS/NUV/MirrorB	None	1200–3300	...	95.6
B 1152+199A	COS/NUV	G230L 2950Å	1650–2050, 2750–3150	1550–2900	7950.4
B 1152+199A	COS/NUV	G230L 3360Å	2059–2458, 3160–3560	1550–2900	1853.3

<sup>a</sup>The spectral resolution increases with the wavelength.

Table 2. Emission Lines Identified in the COS UV Spectrum.

Line	Redshift	Rest-Frame FWHM km s <sup>-1</sup>	Flux 10 <sup>-14</sup> erg cm <sup>-2</sup> s <sup>-1</sup>
C III	1.0155	3458±1080	1.4±0.4
Lyβ	... <sup>a</sup>	... <sup>b</sup>	3.1±0.7
O VI	...	1490±380	2.15±0.63
Lyα	...	6366±1900	11.8±2.8
Lyα	...	1517±846	5.2±2.8
N V	...	2685±1365	2.6±1.0
Si IV	...	894±661	0.3±0.2
C IV	...	6978±1066	10.4±1.4
C IV	...	1431±480	3.4±1.2

<sup>a</sup>The redshifts of all emission lines are linked.

<sup>b</sup>The line width of Lyβ is fixed to be the same as that of the broad Lyα line.

Table 3. Absorption Line Candidates in the COS UV Spectrum.

Line	Wavelength Å	Identification	redshift	Wavelength Å	FWHM km s <sup>-1</sup>	Velocity Dispersion (Rest) km s <sup>-1</sup>	Optical Depth	Column Density 10 <sup>14</sup> cm <sup>-2</sup>
Abs1	1872.3±0.9	O I	... <sup>a</sup>	... <sup>a</sup>	... <sup>a</sup>	...	0.96 <sup>+0.98</sup> <sub>-0.47</sub>	90 <sup>b</sup>
Abs2	1917.7±2.1	C II	0.4377	1915.7±1.0	590 <sup>+450</sup> <sub>-190</sub>	140 <sup>+260</sup> <sub>-40</sub>	0.41 <sup>+0.53</sup> <sub>-0.35</sub>	30
...	...	Lyα	... <sup>a</sup>	... <sup>a</sup>	... <sup>a</sup>	...	< 0.5	< 6.5
Abs3	2226.8±1.4	Lyα(or C IV)	0.8317 (or 0.4377)	2226.8±3.3	280 <sup>+390</sup> <sub>-270</sub>	< 100	0.98 <sup>+8</sup> <sub>-0.48</sub>	8.2
Abs4	2265.8±3.4	Lyα	0.8639	2265.8±3.7	930 <sup>+1270</sup> <sub>-540</sub>	200 <sup>+400</sup> <sub>-60</sub>	0.37 <sup>+0.45</sup> <sub>-0.27</sub>	23

<sup>a</sup>The redshifts, wavelengths, and widths of O I and Lyα lines at  $z = 0.4377$  are linked to those of the C II line.

<sup>b</sup>The spectral bin size of 1.5Å is modeled in calculating the column densities.

acquisition image with *Sherpa* using two Gaussian components (A1 and A2) for the double-image of image A and a constant background, and obtained an acceptable fit. We then added two additional Gaussian components (B1 and B2) for the double-image of image B to the model. The relative position between B1 and A1 is set by previous *HST* measurements (Rusin et al. 2002), and the FWHMs, relative position, and flux ratio between B2 and B1 are set to be the same as those for A2 and A1. Essentially, we added one free parameter to the model, the normalization of B1. We constrained the  $3\sigma$  upper limit of the flux ratio between image B and A as  $f_B/f_A < 100$ . Based on the differential extinction measurement of  $\Delta E(B - V) = 1.20 \pm 0.05$  between images A and B with  $R_V = 2.1 \pm 0.1$  (Elíasdóttir et al. 2006), we expect that image B is fainter than image A by 9–10 mag in the NUV band, consistent with our flux ratio limit.

#### 4. Spectral Analysis

Figure 1 shows the background subtracted NUV spectrum (binned by  $5\text{\AA}$ ) of B 1152+199, a typical broad line quasar spectrum. Since image B is expected to be 9–10 mag fainter than image A in the NUV band, the spectrum is essentially that of image A. The actual spectral fitting was performed on the observed spectrum binned by  $1.5\text{\AA}$  (Figure 4), slightly larger than the resolution limit of  $1\text{\AA}$  of the observation. We also used *Sherpa* to model the spectrum, and we first empirically fit the spectrum using a polynomial continuum model plus nine Gaussian emission lines. We found that a six-component polynomial is sufficient to model the continuum, and the nine detected quasar emission lines are the broad C III, Ly $\beta$ , O VI, Ly $\alpha$ , N V, Si IV, and C IV lines along with narrower components for the Ly $\alpha$  and C IV lines. We set the width of the broad Ly $\alpha$  and Ly $\beta$  lines to be the same in all the fits. We linked the wavelengths of these lines and jointly fit the redshift of the quasar as  $z_s = 1.0155 \pm 0.0013$ . Table 2 lists the emission line properties. There is a multiplicative factor of 0.9966 offset or a linear shift of  $-3.56\text{\AA}$  (observed frame) compared to the quasar redshift,  $z_s = 1.0189 \pm 0.0004$ , measured by Keck II LRIS in the optical band (Myers et al. 1999), reflecting the systematic uncertainties between the two systems.

We next searched for absorption lines in the spectrum. The most significant feature (non-feature) of the spectrum in the absorption regime is the lack of any strong Ly $\alpha$  absorption associated with the lens galaxy (Figure 2). Based on the extinction and X-ray absorption measurements of B 1152+199, we expect a neutral hydrogen column density of  $N_H \sim 10^{20} \text{ cm}^{-2}$  for image A from the lens galaxy, which would result in a damped Ly $\alpha$  line. However, no absorption line is detected at the expected wavelengths 1745–1750 $\text{\AA}$  assuming that the lens redshift is between  $z_l = 0.436$ – $0.439$ . We estimated an upper limit on

the neutral hydrogen column density by modeling the 1720–1770Å spectral segment by a power-law modified by a Voigt absorption profile. We assumed an intrinsic velocity dispersion of  $200 \text{ km s}^{-1}$  at the rest-frame of the absorber, a typical value for normal galaxies, for the Gaussian component, and the absorbed model was further smoothed by the 1.5Å bin size of the observed spectrum. The 68%, 90%, and 99% confidence limits on the neutral hydrogen column density are  $N_{\text{H}} < 0.65, 1.6, \text{ and } 20 \times 10^{15} \text{ cm}^{-2}$ , respectively.

After searching for other absorption lines in the spectrum, we identified four candidates (Abs1–4) at wavelengths 1872.3Å, 1917.7Å, 2226.8Å, and 2265.8Å, respectively. Possible origins of these lines include metal absorption lines associated with the lens galaxy, our own Galaxy, quasar host galaxy, or other Ly $\alpha$  absorbers along the line of sight. We first excluded Galactic absorption lines because the wavelengths do not match any strong UV ISM absorption lines (Blades et al. 1988). We next considered absorption lines in the quasar host galaxy, in particular a series of Fe II absorption lines with rest-wavelengths shorter than that of Ly $\alpha$  will fall in the observed wavelength range; however, they also do not match the wavelengths of the absorption line candidates. Thus, we concluded that Abs1–4 are due to some intervening systems, either the lens galaxy or other intervening clouds. Considering the redshift of the lens ( $z_l \simeq 0.439$ ), Abs1 and Abs2 can be identified as the O I  $\lambda\lambda 1302$  and C II  $\lambda\lambda 1334$  absorption lines from the lens galaxy. Abs3 is located at the wavelength of the expected C IV  $\lambda\lambda 1549$  absorption line from the lens galaxy; however, since we do not expect to have high ionization ions in cold/warm ISM with  $T < 5000\text{K}$ , we excluded C IV from the lens as the interpretation of Abs3 and think it is possibly a Ly $\alpha$  line from a different redshift at  $z = 0.8317$ . Abs4 does not correspond to any strong absorption lines in the lens, and we identified it as another Ly $\alpha$  absorber at  $z = 0.8639$ . We align the O I, and C II absorption lines and the expected DLA from the lensing galaxy together in Figure 3 to further illustrate the non-detection of the expected DLA feature.

We performed a final fit to the spectrum by linking the wavelengths and FWHMs of Abs1 and Abs2, since they are both from the lens galaxy, and reported the best-fit parameters in Table 3. The spectrum, model, and residuals of this fit are shown in Figure 4. We measured the redshift of the lens as  $z_l = 0.4377 \pm 0.0007$ , a multiplicative factor of 0.9971 or a linear shift of  $-1.71\text{Å}$  (observed frame) compared to the Myers et al. (1999) value. To accurately assess the significance of the detections of the O I and C II lines, we calculated a number of confidence intervals and report the one such that the corresponding optical depth is consistent with zero. The O I line is detected by  $2.84\sigma$  (99.77% one-sided probability) and the C II line is detected by  $1.21\sigma$  (88.69% one-sided probability). Considered jointly, the presence of NUV metal absorption lines from the lens galaxy is significant at the 99.975% confidence ( $3.5\sigma$ ) level. We also calculated the rest-frame velocity dispersions of the absorption lines by subtracting the spectral resolution of  $\simeq 1\text{Å}$  in quadrature, and report

the values in Table 3. Although having large uncertainties, the lens velocity dispersion is constrained to be  $140_{-40}^{+260}$  km s<sup>-1</sup>, consistent with values of typical  $L^*$  galaxies.

## 5. Discussion

We have analyzed a COS NUV spectrum of image A of the gravitational lens B 1152+199. We expected to find, based on the absorption seen in the X-ray spectrum, a DLA feature at the lens redshift with  $N_{\text{H}} \sim 10^{20}$  cm<sup>-2</sup> for image A (Dai & Kochanek 2009; Chen et al. 2013). We can place a 99% upper limit on the neutral hydrogen column density with  $N_{\text{H}} < 2 \times 10^{16}$  cm<sup>-2</sup>. We do detect weak O I and C II absorption lines associated with the lens galaxy at a combined significance of  $3.5\sigma$ . B 1152+199 has been well studied in the optical and X-ray bands, and there are multiple indicators showing that B 1152+199 contains a large amount of ISM, the optical extinction, X-ray absorption, and the presence of Mg II and Mg I absorption lines. These previous measurements are consistent with our detection of O I and C II absorption lines. The non-detection of the DLA feature is surprising, and thus, the lens galaxy of B 1152+199 is identified as a “ghostly” DLA, a DLA revealed by other absorption features but undetected (Fathivavsari et al. 2016). Here, we discuss several possible explanations.

First, it is unlikely that the lens has an extremely high metal-to-gas ratio, such that we only detect absorption signatures from the metals or dusts including the extinction, X-ray absorption, and metal absorption lines. Our 99%  $N_{\text{H}}$  upper limit is four orders of magnitude below the expectation, and such an extreme metal-to-gas ratio is unprecedented. Physically, collisions will always bind and mix the atom/molecules of difference species, and creating a region devoid of hydrogen atoms but with only metals is difficult. Second, it is also unlikely that most hydrogen atoms are in the ionized state because of the signatures of cold ISM detected, the O I, C II, Mg I, and Mg II lines. In particular, the ionization potential for Mg I is 7.64 eV lower than that for H I (13.6 eV) and the ionization potential for O I (13.62 eV) is comparable to that of H I, while the O and Mg abundances are much lower. The O I column density is measured to be  $\sim 9 \times 10^{15}$  cm<sup>-2</sup> for image A, and for Solar metallicity, the expected H I column density is  $\sim 10^{19}$  cm<sup>-2</sup>, three orders of magnitude above our 99% limit. Thus, it is difficult to attribute the weak metal absorbers to a satellite galaxy associated with the lens. Image B has  $N_{\text{H}} = 4.8 \times 10^{22}$  cm<sup>-2</sup> from the X-ray spectrum, and this large amount of ISM is consistent with a late-type  $L^*$  galaxy and is difficult to explain it in a satellite as well.

A more plausible explanation is that the expected DLA absorption trough is filled by the Ly $\alpha$  emission from the lens galaxy. Fathivavsari et al. (2016) recently reported another

ghostly DLA system at  $z = 1.70465$  along the line of sight of a  $z = 1.70441$  quasar, and the presence of DLA was also revealed by other metal absorbers. In this case, the DLA and the quasar are very close, and the DLA trough is filled by the Ly $\alpha$  emission from the quasar broad line region. The authors also assumed that the ghostly DLA is falling towards the quasars, which yields an additional redshift such that its measured redshift is larger than that of the quasar. In B 1152+199, the lens galaxy is well separated from the background quasar, and the trough is presumably filled by the Ly $\alpha$  emission from the lens galaxy, and thus the ghostly DLA in B 1152+199 represents a different population. Ly $\alpha$  emission from DLA systems has been detected (e.g., Joshi et al. 2016), usually in the red wing of the DLA absorption profile. The selection method for typical DLAs, however, will miss the B 1152+199-like ghostly DLAs. The Ly $\alpha$  emission usually has a double-humped emission profile to escape from the galaxy (e.g., Hansen & Oh 2006; Dijkstra 2014), and in B 1152+199 it is possible that the DLA trough is filled by the wings of the double-humped emission profile. Depending on the detailed scattering conditions, the two peaks can be separated by up to a few or more Gaussian widths (e.g., Figure 5 of Dijkstra 2014), and the total profile can be broad and shallow. The estimated Ly $\alpha$  luminosity to fill the absorption trough is  $4 \times 10^{42}$  erg s $^{-1}$ , which is close to the break luminosity of the Ly $\alpha$  emitter luminosity function (e.g., Dressler et al. 2015). Higher signal-to-noise ratio and resolution spectrum of B 1152+199 is needed to investigate the details.

Regardless of the explanations, the expected DLA is not detected in B 1152+199, where a large amount of H I is expected. DLAs are important probes to study the baryon distribution in the high redshift universe (e.g., Wolfe et al. 2005). Therefore, it is important to characterize the statistical properties of the B 1152+199-like ghostly DLAs to evaluate the potential biases introduced by these systems.

We acknowledge C.S. Kochanek for helpful comments and C. Fassnacht for providing more details on the Keck II LRIS spectrum of B 1152+199. Support for the program, HST-GO-13283, was provided by NASA through a grant from the Space Telescope Science Institute, which is operated by the Association of Universities for Research in Astronomy, Inc., under NASA contract NAS 5-26555.

## REFERENCES

- Bohlin, R. C., Savage, B. D., & Drake, J. F. 1978, *ApJ*, 224, 132
- Blades, J. C., Wheatley, J. M., Panagia, N., et al. 1988, *ApJ*, 334, 308

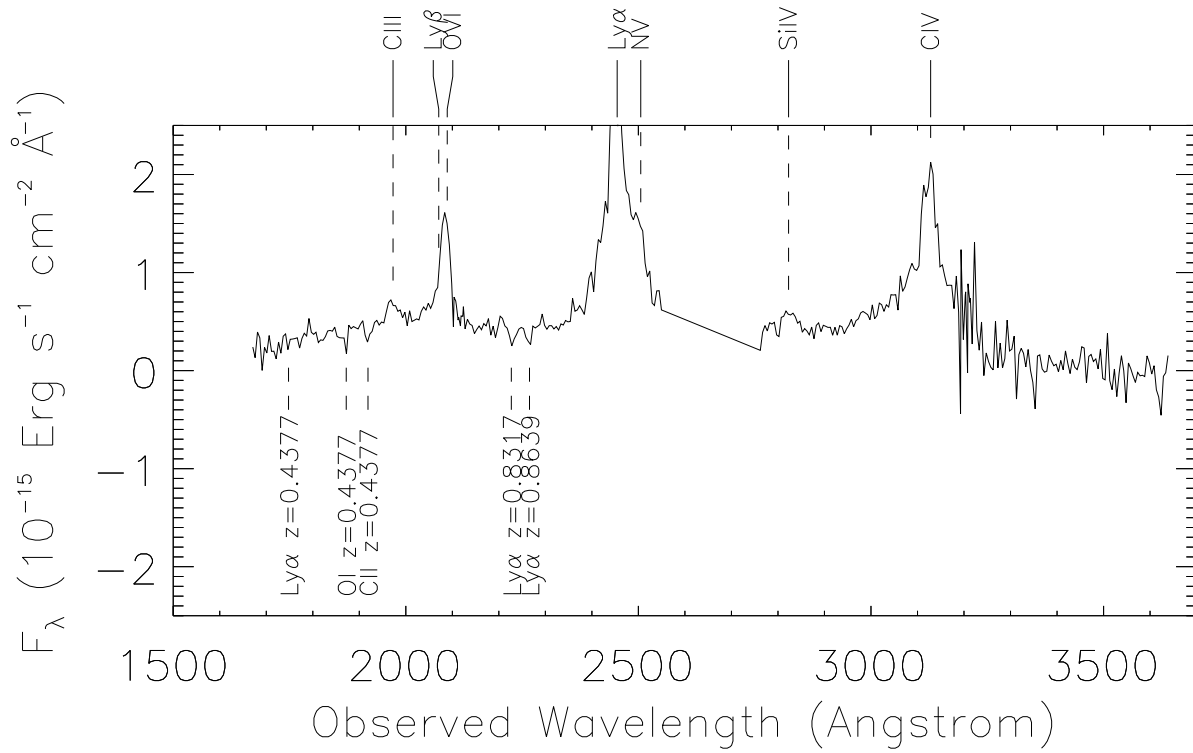


Fig. 1.— *HST*-COS-G230L NUV spectrum of B 1152+199, binned by 5Å. C III, Ly $\beta$ , O VI, Ly $\alpha$ , N v, Si IV, and C IV emission lines from the background quasar at  $z_s = 1.0155$  are labeled on top of the spectrum. The expected strong Ly $\alpha$  absorption feature from the lens galaxy  $z_l = 0.4377$  is not detected. Four low significance absorption lines are detected: two of them are O I and C II absorption lines associated with the lens galaxy, and the other two are other Ly $\alpha$  absorbers along the line of sight at different redshifts.

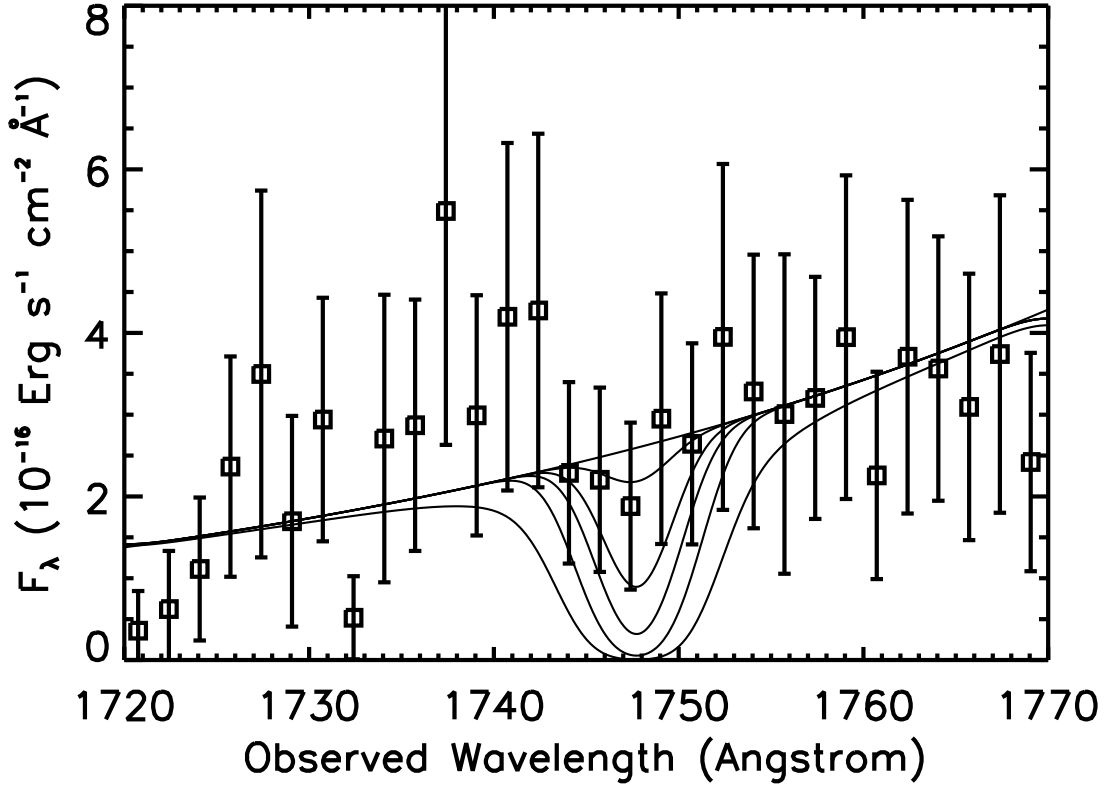


Fig. 2.— The NUV spectrum (squares) between 1720–1770Å of B 1152+199. A DLA system was expected at 1748.8Å (observed frame), which is not detected in the spectrum. The solid curves show a power law model absorbed by Voigt profiles with  $N_{\text{H}} = 0, 10^{14}, 10^{15}, 10^{16}, 10^{18}, 10^{20} \text{ cm}^{-2}$ , from the top to the bottom, further smoothed by the 1.5Å resolution of the spectrum. We measured a  $1\sigma$  upper limit for the neutral hydrogen column density of  $N_{\text{H}} < 6.5 \times 10^{14} \text{ cm}^{-2}$ .

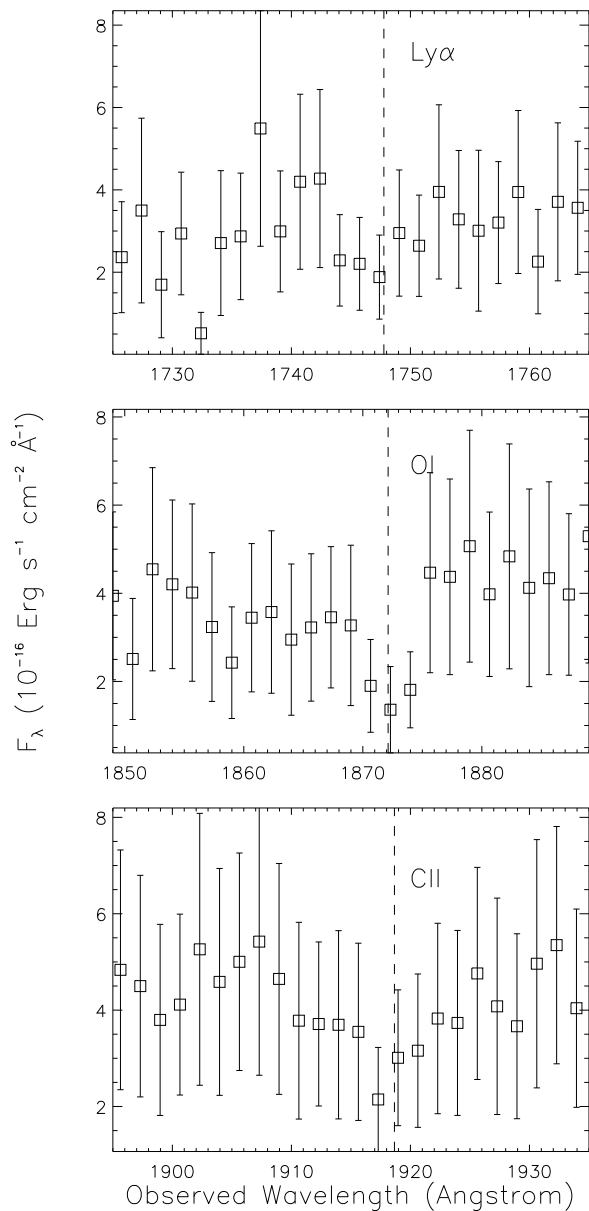


Fig. 3.— Zoomed in NUV spectrum of B 1152+199 close to the absorbers associated with the lens galaxy. The top panel shows the non-detection of the expected Ly $\alpha$  absorption. The middle and bottom panels show the O I and C II lines from the lens galaxy. The vertical lines show the expected wavelengths of these lines for a lens redshift of  $z_l = 0.4377$ .

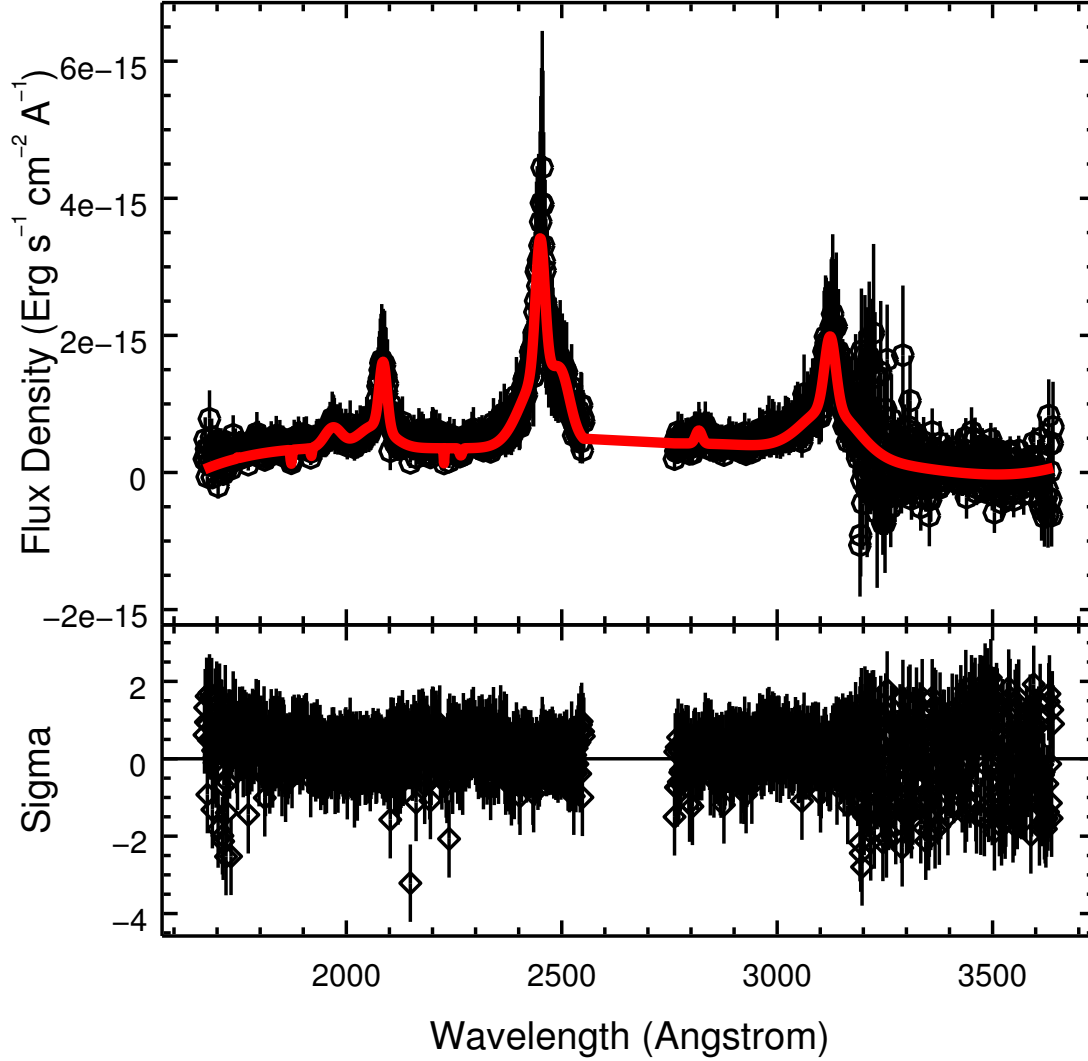


Fig. 4.— *HST*-COS-G230L NUV spectrum of B 1152+199, binned by  $1.5\text{\AA}$ , and its best-fit model (red line). The model is composed of a six-component polynomial for the continuum emission, nine emission lines from the background quasar (C III,  $\text{Ly}\beta$ , O VI, broad and narrower  $\text{Ly}\alpha$ , N V, Si IV, and broad and narrower C IV lines), and five absorption systems.

- Chen, B., Dai, X., Kochanek, C. S., & Chartas, G. 2013, arXiv:1306.0008
- Dai, X., Chartas, G., Agol, E., Bautz, M. W., & Garmire, G. P. 2003, *ApJ*, 589, 100
- Dai, X., & Kochanek, C. S. 2005, *ApJ*, 625, 633
- Dai, X., Kochanek, C. S., Chartas, G., & Mathur, S. 2006, *ApJ*, 637, 53
- Dai, X., & Kochanek, C. S. 2009, *ApJ*, 692, 677
- Dijkstra, M. 2014, *PASA*, 31, e040
- Dressler, A., Henry, A., Martin, C. L., et al. 2015, *ApJ*, 806, 19
- Elíasdóttir, Á., Hjorth, J., Toft, S., Burud, I., & Paraficz, D. 2006, *ApJS*, 166, 443
- Falco, E. E., Impey, C. D., Kochanek, C. S., et al. 1999, *ApJ*, 523, 617
- Fathivavsari, H., Petitjean, P., Zou, S., et al. 2016, arXiv:1611.05421
- Green, J. C., Froning, C. S., Osterman, S., et al. 2012, *ApJ*, 744, 60
- Hansen, M., & Oh, S. P. 2006, *MNRAS*, 367, 979
- Joshi, R., Srianand, R., Noterdaeme, P., & Petitjean, P. 2016, arXiv:1610.06580
- Mediavilla, E., Muñoz, J. A., Kochanek, C. S., et al. 2005, *ApJ*, 619, 749
- Ménard, B., & Chelouche, D. 2009, *MNRAS*, 393, 808
- Motta, V., Mediavilla, E., Muñoz, J. A., et al. 2002, *ApJ*, 574, 719
- Myers, S. T., et al. 1999, *AJ*, 117, 2565
- Muñoz, J. A., Falco, E. E., Kochanek, C. S., McLeod, B. A., & Mediavilla, E. 2004, *ApJ*, 605, 614
- Nadeau, D., Yee, H. K. C., Forrest, W. J., et al. 1991, *ApJ*, 376, 430
- Oguri, M., & Marshall, P. J. 2010, *MNRAS*, 405, 2579
- Prochaska, J. X., & Herbert-Fort, S. 2004, *PASP*, 116, 622
- Rusin, D., Norbury, M., Biggs, A. D., et al. 2002, *MNRAS*, 330, 205
- Toft, S., Hjorth, J., & Burud, I. 2000, *A&A*, 357, 115

Wolfe, A. M., Gawiser, E., & Prochaska, J. X. 2005, *ARA&A*, 43, 861

Wucknitz, O., Wisotzki, L., Lopez, S., & Gregg, M. D. 2003, *A&A*, 405, 445